articles

molecular pharmaceutics

Superparamagnetic Iron Oxide Nanotheranostics for Targeted Cancer Cell Imaging and pH-Dependent Intracellular Drug Release

Peng Zou,[†] Yanke Yu,[†] Y. Andrew Wang,[‡] Yanqiang Zhong,[§] Amanda Welton,[||] Craig Galbán,[||] Shaomeng Wang,[⊥] and Duxin Sun*,[†]

Department of Pharmaceutical Sciences, College of Pharmacy, University of Michigan, Ann Arbor, Michigan 48109, Ocean NanoTech, LLC700 Research Center Boulevard, Fayetteville, Arkansas 72701, Department of Pharmaceutics, College of Pharmacy, Second Military Medical University, Shanghai, 200433, China, Department of Radiology, University of Michigan, Ann Arbor, Michigan 48109, and Comprehensive Cancer Center, Departments of Internal Medicine, Pharmacology and Medicinal Chemistry, University of Michigan, Ann Arbor, Michigan 48109

Received August 17, 2010; Revised Manuscript Received September 15, 2010; Accepted September 16, 2010

Abstract: Studies were conducted to develop antibody- and fluorescence-labeled superparamagnetic iron oxide nanoparticle (SPIO) nanotheranostics for magnetic resonance imaging (MRI) and fluorescence imaging of cancer cells and pH-dependent intracellular drug release. SPIO nanoparticles (10 nm) were coated with amphiphilic polymers and PEGylated. The antibody HuCC49ΔCH2 and fluorescent dye 5-FAM were conjugated to the PEG of iron oxide nanoparticles (IONPs). Anticancer drugs doxorubicin (Dox), azido-doxorubicin (Adox), MI-219, and 17-DMAG containing primary amine, azide, secondary amine, and tertiary amine, respectively, were encapsulated into IONPs. The encapsulation efficiency and drug release at various pHs were determined using LC−MS/MS. The cancer targeting and imaging were monitored using MRI and fluorescent microscopy in a colon cancer cell line (LS174T). The pH-dependent drug release, intracellular distribution, and cytotoxicity were evaluated using microscopy and MTS assay. The PEGylation of SPIO and conjugation with antibody and 5-FAM increased SPIO size from 18 to 44 nm. Fluorescent imaging, magnetic resonance imaging (MRI) and Prussian blue staining demonstrated that HuCC49ΔCH2-SPIO increased cancer cell targeting. HuCC49ΔCH2-SPIO nanotheranostics decreased the T_2 values in MRI of LS174T cells from 117.3 ± 1.8 ms to 55.5 ± 2.6 ms. The loading capacities of Dox, Adox, MI-219, and 17-DMAG were 3.16 ± 0.77%, 6.04 ± 0.61%, 2.22 ± 0.42%, and 0.09 ± 0.07%, respectively. Dox, MI-219 and 17-DMAG showed pH-dependent release while Adox did not. Fluorescent imaging demonstrated the accumulation of HuCC49ΔCH2-SPIO nanotheranostics in endosomes/lysosomes. The encapsulated Dox was released in acidic lysosomes and diffused into cytosol and nuclei. In contrast, the encapsulated Adox only showed limited release in endosomes/lysosomes. HuCC49ΔCH2-SPIO nanotheranostics target-delivered more Dox to LS174T cells than nonspecific IgG-SPIO and resulted in a lower IC_{50} (1.44 μM vs 0.44 μM). The developed HuCC49ΔCH2-SPIO nanotheranostics provides an integrated platform for cancer cell imaging, targeted anticancer drug delivery and pH-dependently drug release.

Keywords: Iron oxide nanoparticle (SPIO); MRI; fluorescent imaging; targeted drug delivery; nanotheranostics; doxorubicin; intracellular drug release

10.1021/mp100273t
Published on Web 09/16/2010

Introduction

One of the major challenges in cancer chemotherapy is the serious side effects caused by cytotoxicity of anticancer drugs. Novel strategies are needed to site-specifically deliver anticancer drugs to tumor cells. Superparamagnetic iron oxide nanoparticles (SPIOs) have emerged as feasible nanotheranostics for tumor imaging and targeted anticancer drug delivery.[1−20] SPIOs are a contrast agent for magnetic resonance imaging (MRI) since they induce a shorter T_2 relaxation (transverse or spin−spin relaxation), producing a decreased signal intensity on a T_2-weighted image.[21] Various SPIO products have been clinically used as contrast agents due to their high contrast effects and biocompatibility.[22] The standard water-soluble SPIOs are composed of an iron-oxide magnetic core coated with hydrophobic oleic acid (OA) and a surface of amphiphilic polymers.[8] The surface polymers not only stabilize the nanoparticles but also provide active

* To whom correspondence should be addressed. Mailing address: Department of Pharmaceutical Sciences, College of Pharmacy, The University of Michigan, 428 Church Street, Ann Arbor, MI 48109. Tel: 734-615-8740. Fax: 734-615-6162. E-mail: duxins@umich.edu.

† Department of Pharmaceutical Sciences, College of Pharmacy, University of Michigan.

‡ Ocean NanoTech.

§ Second Military Medical University.

|| Department of Radiology, University of Michigan.

⊥ Comprehensive Cancer Center, Departments of Internal Medicine, Pharmacology and Medicinal Chemistry, University of Michigan.

(1) Yu, M. K.; Jeong, Y. Y.; Park, J.; Park, S.; Kim, J. W.; Min, J. J.; Kim, K.; Jon, S. Drug-loaded superparamagnetic iron oxide nanoparticles for combined cancer imaging and therapy in vivo. *Angew. Chem., Int. Ed.* **2008**, *47* (29), 5362–5365.

(2) Yang, L. L.; Cao, Z. H.; Sajja, H. K.; Mao, H.; Wang, L. Y.; Geng, H. Y.; Xu, H. Y.; Jiang, T. S.; Wood, W. C.; Nie, S. M.; Wang, Y. A. Development of Receptor Targeted Magnetic Iron Oxide Nanoparticles for Efficient Drug Delivery and Tumor Imaging. *J. Biomed. Nanotechnol.* **2008**, *4* (4), 439–449.

(3) Yang, L. L.; Mao, H.; Wang, Y. A.; Cao, Z. H.; Peng, X. H.; Wang, X. X.; Duan, H. W.; Ni, C. C.; Yuan, Q. G.; Adams, G.; Smith, M. Q.; Wood, W. C.; Gao, X. H.; Nie, S. M. Single Chain Epidermal Growth Factor Receptor Antibody Conjugated Nanoparticles for in vivo Tumor Targeting and Imaging. *Small* **2009**, *5* (2), 235–243.

(4) Maeng, J. H.; Lee, D. H.; Jung, K. H.; Bae, Y. H.; Park, I. S.; Jeong, S.; Jeon, Y. S.; Shim, C. K.; Kim, W.; Kim, J.; Lee, J.; Lee, Y. M.; Kim, J. H.; Kim, W. H.; Hong, S. S. Multifunctional doxorubicin loaded superparamagnetic iron oxide nanoparticles for chemotherapy and magnetic resonance imaging in liver cancer. *Biomaterials* **2010**, *31* (18), 4995–5006.

(5) Kumar, A.; Jena, P. K.; Behera, S.; Lockey, R. F.; Mohapatra, S. Multifunctional magnetic nanoparticles for targeted delivery. *Nanomedicine* **2010**, *6* (1), 64–69.

(6) Chertok, B.; Moffat, B. A.; David, A. E.; Yu, F. Q.; Bergemann, C.; Ross, B. D.; Yang, V. C. Iron oxide nanoparticles as a drug delivery vehicle for MRI monitored magnetic targeting of brain tumors. *Biomaterials* **2008**, *29* (4), 487–496.

(7) Munnier, E.; Cohen-Jonathan, S.; Linassier, C.; Douziech-Eyrolles, L.; Marchais, H.; Souce, M.; Herve, K.; Dubois, P.; Chourpa, I. Novel method of doxorubicin-SPION reversible association for magnetic drug targeting. *Int. J. Pharm.* **2008**, *363* (1−2), 170–176.

(8) Jain, T. K.; Morales, M. A.; Sahoo, S. K.; Leslie-Pelecky, D. L.; Labhasetwar, V. Iron oxide nanoparticles for sustained delivery of anticancer agents. *Mol. Pharmaceutics* **2005**, *2* (3), 194–205.

(9) Jain, T. K.; Reddy, M. K.; Morales, M. A.; Leslie-Pelecky, D. L.; Labhasetwar, V. Biodistribution, clearance, and biocompatibility of iron oxide magnetic nanoparticles in rats. *Mol. Pharmaceutics* **2008**, *5* (2), 316–327.

(10) Jain, T. K.; Richey, J.; Strand, M.; Leslie-Pelecky, D. L.; Flask, C. A.; Labhasetwar, V. Magnetic nanoparticles with dual functional properties: drug delivery and magnetic resonance imaging. *Biomaterials* **2008**, *29* (29), 4012–4021.

(11) Das, M.; Mishra, D.; Dhak, P.; Gupta, S.; Maiti, T. K.; Basak, A.; Pramanik, P. Biofunctionalized, phosphonate-grafted, ultrasmall iron oxide nanoparticles for combined targeted cancer therapy and multimodal imaging. *Small* **2009**, *5* (24), 2883–2893.

(12) Yang, Y.; Jiang, J. S.; Du, B.; Gan, Z. F.; Qian, M.; Zhang, P. Preparation and properties of a novel drug delivery system with both magnetic and biomolecular targeting. *J. Mater. Sci.: Mater. Med.* **2009**, *20* (1), 301–307.

(13) Nasongkla, N.; Bey, E.; Ren, J. M.; Ai, H.; Khemtong, C.; Guthi, J. S.; Chin, S. F.; Sherry, A. D.; Boothman, D. A.; Gao, J. M. Multifunctional polymeric micelles as cancer-targeted, MRI-ultrasensitive drug delivery systems. *Nano Lett.* **2006**, *6* (11), 2427–2430.

(14) Jain, T. K.; Foy, S. P.; Erokwu, B.; Dimitrijevic, S.; Flask, C. A.; Labhasetwar, V. Magnetic resonance imaging of multifunctional pluronic stabilized iron-oxide nanoparticles in tumor-bearing mice. *Biomaterials* **2009**, *30* (35), 6748–6756.

(15) Liu, S. J.; Jia, B.; Qiao, R. R.; Yang, Z.; Yu, Z. L.; Liu, Z. F.; Liu, K.; Shi, J. Y.; Han, O. Y.; Wang, F.; Gao, M. Y. A Novel Type of Dual-Modality Molecular Probe for MR and Nuclear Imaging of Tumor: Preparation, Characterization and in Vivo Application. *Mol. Pharmaceutics* **2009**, *6* (4), 1074–1082.

(16) Hafelli, U. O.; Riffle, J. S.; Harris-Shekhawat, L.; Carmichael-Baranauskas, A.; Mark, F.; Dailey, J. P.; Bardenstein, D. Cell Uptake and in Vitro Toxicity of Magnetic Nanoparticles Suitable for Drug Delivery. *Mol. Pharmaceutics* **2009**, *6* (5), 1417–1428.

(17) Talelli, M.; Rijcken, C. J. F.; Lammers, T.; Seevinck, P. R.; Storm, G.; van Nostrum, C. F.; Hennink, W. E. Superparamagnetic Iron Oxide Nanoparticles Encapsulated in Biodegradable Thermosensitive Polymeric Micelles: Toward a Targeted Nanomedicine Suitable for Image-Guided Drug Delivery. *Langmuir* **2009**, *25* (4), 2060–2067.

(18) Guthi, J. S.; Yang, S. G.; Huang, G.; Li, S. Z.; Khemtong, C.; Kessinger, C. W.; Peyton, M.; Minna, J. D.; Brown, K. C.; Gao, J. M. MRI-Visible Micellar Nanomedicine for Targeted Drug Delivery to Lung Cancer Cells. *Mol. Pharmaceutics* **2010**, *7* (1), 32–40.

(19) Wang, B. D.; Xu, C. J.; Xie, J.; Yang, Z. Y.; Sun, S. L. pH Controlled Release of Chromone from Chromone-Fe_3O_4 Nanoparticles. *J. Am. Chem. Soc.* **2008**, *130* (44), 14436–14437.

(20) Rao, K. S.; Reddy, M. K.; Horning, J. L.; Labhasetwar, V. TAT-conjugated nanoparticles for the CNS delivery of anti-HIV drugs. *Biomaterials* **2008**, *29* (33), 4429–4438.

(21) Yanke Yu, D. S. Superparamagnetic iron oxide nanoparticle 'theranostics' for multimodality tumor imaging, gene delivery, targeted drug and prodrug delivery. *Expert Rev. Clin. Pharmacol.* **2010**, *3* (1), 117–130.

(22) Wang, Y. X.; Hussain, S. M.; Krestin, G. P. Superparamagnetic iron oxide contrast agents: physicochemical characteristics and applications in MR imaging. *Eur. Radiol.* **2001**, *11* (11), 2319–2331.

functional groups for controllable bioconjugation of targeting ligands. Furthermore, surface coating with biocompatible polymers such as PEG can reduce reticuloendothelial system (RES) uptake of SPIOs as well as nonspecific interaction with plasma membranes. It has been demonstrated that the cancer-targeting ligand labeled SPIOs could specifically bind to cancer cells and accumulate in tumor tissues.[1−3,10,18]

SPIOs have been utilized as a carrier for targeted drug delivery.[1,2,6,8,20,23] Drug molecules were either entrapped in the SPIO surface polymer layer using physical interactions (electrostatic interaction or hydrophobic interaction) or covalently conjugated to the functional groups on SPIO surface for pH-dependent release or enzymatic cleavage release in targeted tissues.[12,24] Doxorubicin (Dox) has been used as a model drug for targeted drug delivery since the hydrophobic compound can partition into the oleic acid shell of SPIOs[8] and its intracellular distribution can be visualized under a fluorescent microscope. Dox has been reported to exhibit pH-dependent release from SPIOs.[2,4,7,12] Approximately 60% of the Dox was released within 50 min at pH 5.1 in acetate buffer.[1]

The reasons for the rapid release of Dox at low pH are still not clear. One explanation was the protonation of the primary amine of Dox which dramatically increased the solubility of Dox in aqueous solution.[2] Another explanation is the weakened interaction between Dox and the partially neutralized carboxyl groups of polymers or oleic acid.[1,4] The pH-dependent release of Dox suggests that Dox may be rapidly released from SPIOs in acidic environment of tumor tissues or endosomes/lysosomes after internalization into cancer cells.

Ideally, nanotheranostics can be used for noninvasive cancer imaging, visualizing drug delivery, assessing the efficiency of targeted drug delivery, and monitoring the therapeutic responses. In this study, we developed tumor-associated glycoprotein-72 (TAG-72) targeted SPIO nanotheranostics for simultaneous MRI and fluorescent imaging of cancer cells and targeted anticancer drug delivery. Our previous studies demonstrated that anti-TAG-72 antibody HuCC49ΔC_H2 could specifically bind to TAG-72 expressing LS174T colon cancer cells *in vitro* and *in vivo*.[25] HuCC49ΔC_H2 and fluorescent dye 5-FAM were conjugated to the carboxyl groups of PEGylated SPIOs. The targeting of the nanotheranostics to LS174T cells was assessed using MRI, fluorescent imaging and Prussian blue staining.

To further study the mechanism of intracellular release of Dox, we prepared azido-doxorubicin (Adox) by replacing the primary amine of Dox with a nonionizable azido group. The intracellular release of Dox and Adox was compared to confirm their release mechanism. An MDM2 inhibitor (MI-219)[26] and an Hsp90 inhibitor (17-DMAG), which have a secondary amine and a tertiary amine, respectively, were used for comparison. The drug-loading capacity and drug release at various pHs among the four compounds were compared. The intracellular localization of SPIOs and pH-dependent drug release in endosomes/lysosomes were visualized by tracking the fluorescence of 5-FAM, Dox and Adox. To our knowledge, our studies first visualized the pH-dependent drug release from SPIOs in endosomes/lysosomes of cancer cells.

Materials and Methods

Materials. SPIOs with a 10 nm iron oxide core (Catalog No. SHP-10-50) and SuperMag Separator were supplied by Ocean NanoTech (Springdale, AR). SPIOs coated with oleic acid and amphiphilic polymer were dissolved in deionized water (5 mg/mL). The oleic acid layer and polymer layer are approximately 2 nm in thickness, respectively. Heterobifunctional PEG polymer (NH2-PEG-COOH) was purchased from JenKem Technology USA Inc. (Allen, TX). 5-FAM cadaverine was purchased from AnaSpec (Fremont, CA). HuCC49ΔCH2 antibody was supplied by National Cancer Institute (Bethesda, MD). Cell culture media and phosphate buffered saline (PBS) were purchased from Invitrogen (Carlsbad, CA). PD-10 desalting columns were purchased from GE Healthcare (Piscataway, NJ). 17-DMAG was purchased from LC Laboratories (Woburn, MA). The nonspecific IgG antibodies from human serum, *N*-(3-Dimethyl aminopropyl)-*N*′-ethylcarbodiimide (EDC), and *N*-hydroxysulfosuccinimide sodium salt (sulfo-NHS), as well as all other chemical reagents, were purchased from Sigma-Aldrich Chemical Co. (St. Louis, MO).

SPIO PEGylation and Conjugation with 5-FAM and Antibodies. A total of 10 mg (9 nmol) of SPIOs was dissovled in 5 mL of borate buffer (pH 5.5). EDC (0.3 mg) and sulfo-NHS (0.4 mg) were added to the mixture and kept stirring to activate the carboxyl on the surface of SPIOs. After 20 min, excess EDC and sulfo-NHS were removed using a desalting column balanced with pH 5.5 borate buffer. HOOC-PEG-NH_2 (MW 2,000, 0.3 g) was added to the eluted SPIO solution with stirring, and immediately the pH was adjusted to >8.0 by addition of 0.5 mL of 30 mM borax solution.

(23) Park, J. H.; von Maltzahn, G.; Ruoslahti, E.; Bhatia, S. N.; Sailor, M. J. Micellar hybrid nanoparticles for simultaneous magnetofluorescent imaging and drug delivery. *Angew. Chem., Int. Ed.* **2008**, *47* (38), 7284–7288.

(24) Wang, A. Z.; Bagalkot, V.; Vasilliou, C. C.; Gu, F.; Alexis, F.; Zhang, L.; Shaikh, M.; Yuet, K.; Cima, M. J.; Langer, R.; Kantoff, P. W.; Bander, N. H.; Jon, S.; Farokhzad, O. C. Superparamagnetic iron oxide nanoparticle-aptamer bioconjugates for combined prostate cancer imaging and therapy. *ChemMedChem* **2008**, *3* (9), 1311–1315.

(25) Zou, P.; Xu, S.; Povoski, S. P.; Wang, A.; Johnson, M. A.; Martin, E. W., Jr.; Subramaniam, V.; Xu, R.; Sun, D. Near-infrared fluorescence labeled anti-TAG-72 monoclonal antibodies for tumor imaging in colorectal cancer xenograft mice. *Mol. Pharmaceutics* **2009**, *6* (2), 428–440.

(26) Shangary, S.; Qin, D.; McEachern, D.; Liu, M.; Miller, R. S.; Qiu, S.; Nikolovska-Coleska, Z.; Ding, K.; Wang, G.; Chen, J.; Bernard, D.; Zhang, J.; Lu, Y.; Gu, Q.; Shah, R. B.; Pienta, K. J.; Ling, X.; Kang, S.; Guo, M.; Sun, Y.; Yang, D.; Wang, S. Temporal activation of p53 by a specific MDM2 inhibitor is selectively toxic to tumors and leads to complete tumor growth inhibition. *Proc. Natl. Acad. Sci. U.S.A.* **2008**, *105* (10), 3933–3938.

Desalting columns were used to remove excess PEG polymers. The PEGylated SPIOs were concentrated using a SuperMag separator and dissolved in pH 5.5 borate buffer for antibody and 5-FAM conjugation.

PEGylated SPIOs (2 mg/mL, 1 mL) were added with 30 μg of EDC and 40 μg of sulfo-NHS and stirred for 20 min. Excess EDC and sulfo-NHS were removed using a desalting column. Antibody (1 mg, HuCC49ΔCH2 or nonspecific IgG in PBS) was added to the eluted solution with stirring. Five minutes later, 0.1 mL of 5-FAM cadaverine (2 mg/mL in 30 mM borax solution) was added to the mixture. The mixture was stirred at 4 °C and in the dark overnight. A PD-10 column was used to remove the excess 5-FAM cadaverine, and SuperMag Separator was used to remove the unlabeled antibody. SPIOs labeled with HuCC49ΔCH2 and 5-FAM were named mAb-SPIOs, and SPIOs labeled with nonspecific human IgG and 5-FAM were named IgG-SPIOs. Similarly, 1 mL of PEGylated SPIOs (2 mg/mL) was labeled with 5-FAM using the amide formation reaction.

Particle Size Determination, Zeta Potential Measurement and Electrophoresis. The hydrodynamic size and zeta-potential of nanoparticles in each preparation step were measured by dynamic laser light scattering (DLS) and M3-PALS technology on a Zetasizer Nano ZS particle sizer (Malvern Instruments Ltd., Westborough, MA), respectively. Each sample was dispersed in deionized water (0.01 mg/mL) using a water-bath sonicator for 2 min and measured in a disposable capillary cell cuvette (Malvern Instruments Ltd., Westborough, MA). Agarose gel electrophoresis was performed to test the migration of the SPIO and its conjugates. Agarose gel (1%) was prepared in 1× TAE buffer. The nanoparticles were mixed with bromophenol blue loading buffer (Sigma, St. Louis, MO), and 20 μL of sample was loaded into each well. The gel was run in 1× TAE buffer at a voltage of 100 V for 1 h.

Cell Culture. Human colon cancer cell line LS174T (TAG-72 positive) and human skin cancer cell line A375 (TAG-72 negative) obtained from American Type Culture Collection (ATCC, Rockville, MD) were cultured in Dulbecco's modified Eagle's high glucose medium (DMEM) supplemented with 10% fetal bovine serum (FBS) and 1% penicillin−streptomycin (Invitrogen Life Technologies, Carlsbad, CA). The cells were maintained in a humidified atmosphere of 5% CO_2 at 37 °C, with the medium changed every other day.

***In Vitro* MRI Scan of Cancer Cells.** MRI scan of cancer cells was carried out as described previously.[11,27,28] Briefly, 5×10^5 LS174T cells per well were seeded in a 6-well plate and allowed to grow for 24 h. Cells were incubated with mAb-SPIOs at a concentration equivalent to 0.03 mg/mL SPIOs at 37 °C for 1 or 4 h. The unlabeled SPIOs and IgG-SPIOs were used as controls. Then cells were washed twice with PBS and digested by 0.25% trypsin. One million of cells were suspended in 1 mL of 1% agarose in 1.5 mL Eppendorf tubes and vortexed for 30 s. After 1% agarose was solidified, samples were then sealed with additional 1% agarose to avoid air susceptibility artifacts. The samples were scanned on a Varian 7T MRI scanner (Varian, Palo Alto, CA). A spin−echo pulse sequence with multiecho acquisitions was selected from the Varian VnmrJ software package to acquire MR phantom images at multiple echo times. Sequence parameters used were as follows: repetition time (TR) of 3000 ms, echo times (TE) of 15−150 ms, echo train length of 6 and echo spacing of 15 ms, respectively. The spatial resolution parameters were set as follows: an acquisition matrix of 128 × 64, field of view of 30 × 30 mm^2, section thickness of 1 mm, and 1 average. The MRI signal intensity (SI) was measured using the Matlab software (MathWorks, Inc., Natick, MA). T_2 values were obtained by plotting the SI of each sample over a range of TE values. T_2 relaxation times were then calculated by fitting a first-order exponential decay curve to the plot. A copper pseudocolor was added to the MR phantom images using Matlab.

Prussian Blue Staining. A total of 1×10^5 LS174T cells were seeded in a 24-well plate and allowed to grow for 24 h. Cells were incubated with mAb-SPIOs, SPIOs and IgG-SPIOs (equivalent to 20 μg/mL of SPIO) at 37 °C for 4 h, washed with PBS twice, and fixed with formaldehyde (2%). Then, the cells were treated with a staining solution containing a 1:1 mixture of 5% potassium ferrocyanide and 5% HCl acid at 37 °C for 1 h. The cells were then examined under an Olympus BX-51 upright light microscope equipped with an Olympus DP-70 high resolution digital camera (Olympus Imaging America Inc., Center Valley, PA).

Fluorescent Microscopy. A total of 2×10^4 LS174T or A375 cells were seeded in a 96-well plate and allowed to grow for 24 h. After incubation with 5-FAM labeled SPIOs, mAb-SPIOs and IgG-SPIOs for 4 h, LS174T or A375 cells were washed and stained with Hoechst (10 μM) at 37 °C for 1 h and imaged using Nikon TE2000S epifluorescence microscope coupled with a standard mercury bulb illumination, a CCD camera (Roper Scientific, Tucson, AZ), a 20× objective, and a triple-pass DAPI/FITC/TRITC filter set (Chroma Technology Corp. 86013v2). The acquired 12-bit grayscale images were background subtracted. The images obtained with DAPI and FITC channels were overlaid using MetaMorph software (Molecular Devices Corporation, Sunnyvale, CA). To visualize the intracellular drug release, LS174T cells were incubated with Dox or Adox loaded mAb-SPIO for 1, 6, and 24 h and their nuclei were stained with Hoechst. The images obtained with DAPI, FITC and TRITC filters were overlaid.

(27) Yang, L.; Mao, H.; Wang, Y. A.; Cao, Z.; Peng, X.; Wang, X.; Duan, H.; Ni, C.; Yuan, Q.; Adams, G.; Smith, M. Q.; Wood, W. C.; Gao, X.; Nie, S. Single chain epidermal growth factor receptor antibody conjugated nanoparticles for in vivo tumor targeting and imaging. *Small* **2009**, *5* (2), 235–243.

(28) Yang, L.; Mao, H.; Cao, Z.; Wang, Y. A.; Peng, X.; Wang, X.; Sajja, H. K.; Wang, L.; Duan, H.; Ni, C.; Staley, C. A.; Wood, W. C.; Gao, X.; Nie, S. Molecular Imaging of Pancreatic Cancer in a Preclinical Animal Tumor Model Using Targeted Multifunctional Nanoparticles. *Gastroenterology* **2009**, *136* (5), 15141525.e2.

Drug Loading and Release. Dox and Adox were synthesized in water-insoluble base form. The hydrochloride salt of 17-DMAG and MI-219 was converted into water-insoluble free base. 5 mg of hydrochloride salt of 17-DMAG or MI-219 was dissolved in 2 mL of 0.1 M sodium carbonate solution and vortexed for 1 min. 17-DMAG or MI-219 in free base was extracted by acetyl acetate (4 mL × 3). Acetyl acetate was evaporated using a Speedvac concentrator (Thermo Scientific, Waltham, MA) to obtain 17-DMAG or MI-219 in free base. Methanol solution (0.13 mL) of the drug in free base (5 mg/mL) was added dropwise with stirring to 2 mL of SPIOs or conjugates (equivalent to 1 mg/mL of SPIOs in pH 8.0 buffer). An air flow was used to evaporate methanol, and the remaining aqueous solution was stirred overnight to allow the drug partition into the oleic acid shell. Drug-loaded SPIOs or conjugates passed through a PD-10 desalting column to remove unencapsulated drug molecules. The eluted SPIO or conjugates were concentrated to 1 mg/mL using a SuperMag Separator. To determine the loading capacity, a 50 μL aliquot of SPIOs or conjugate suspension was diluted with methanol (1 mL), sonicated for 1 min and centrifuged at 21000*g* for 30 min to spin down nanoparticles. The supernatant was diluted with methanol and injected on a LC−MS/MS to quantify the amount of released drug. To test pH-dependent drug release, a 50 μL aliquot of SPIOs or conjugate solution was suspended in 0.95 mL of a series of HOAc/NH_4OAc/NH_4OH buffers at pH 3.21, 4.19, 4.95, 5.66, 6.65, and 7.21. After incubation for 1 or 24 h, the buffer solutions were centrifuged at 21000*g* for 30 min and the supernatant was further diluted with methanol before LC−MS/MS analysis. The percentages of drug release at various pHs were calculated as the ratios of the amount of released drug in buffers and methanol. LogP of MI-219 was predicted by using MarvinSketch from ChemAxon (Budapest, Hungary).

LC−MS/MS Analysis. LC−MS/MS analysis was performed on an Agilent 1200 HPLC system and a Qtrap 3200 mass spectrometer (Applied Biosystems, MDS Sciex Toronto, Canada) equipped with an electrospray ionization (ESI) source. Aliquots (10 μL) were injected onto a reversed-phase Zorbax Bonus-RP column (5 cm × 2.1 mm i.d., 3.5 μm) (Agilent, Santa Clara, CA). The mobile phase consisted of 0.1% formic acid in water (A) and 0.1% formic acid in methanol (B). The mobile phase A was held at 10% for 1.0 min, linearly increased from 10% to 90% over 0.1 min, held at 90% for an additional 2 min, and then immediately stepped back down to 10 for re-equilibration. The mobile phase flow rate was 0.4 mL/min. Quantification of Dox and 17-DMAG was performed by using positive multiple reaction monitoring (MRM) scan of the $[M + H]^+$ ions and the product ions of each compound. The MRM transition channels were 544/361 and 617/58 respectively. The collision energy was set as 39 and 67, respectively. Adox and MI-219 were quantified using negative MRM scan, and transition channels were 568/395 and 550/306, respectively. The collision energy was −18 for Adox and −38 for MI-219. HPLC and mass spectrometric parameters are optimized by using sample infusion and flow injection analysis (FIA).

MTS Assay. LS174T cells were seeded at 4000 per well in 96-well plates 24 h prior to the experiment. A series of solutions of Dox or Dox-loaded nanoparticles (mAb-SPIOs and SPIOs) were prepared in DMEM media and added to the wells. The final concentrations of Dox ranged from 0.01 μM to 5 μM. Adox and Adox loaded nanoparticles were dissolved in DMEM media and incubated with LS174T cells. The final concentrations of Adox ranged from 0.01 μM to 20 μM. SPIOs without drug and blank medium were used as controls. Cell viability was determined after incubation for 4 days. The absorption of the cells in each well at 490 nm was measured using a plate reader before and after incubation with MTS and PMS (Promega, Madison, WI) for 2 h. The first measured absorption was subtracted from the second measured absorption to minimize the errors caused by the absorption of SPIOs at 490 nm. The effect of drug on cell proliferation was calculated as the percentage of inhibition in cell growth with respect to the controls. IC_{50} values were calculated using WinNonlin Version 5.2.1 (Pharsight, Mountain View, CA).

Results

Conjugation and Physical Characterization of Antibody Labeled SPIOs. Figure 1 shows the schematic production of HuCC49ΔCH2 labeled SPIOs (mAb-SPIOs) or nonspecific IgG labeled SPIOs (IgG-SPIOs). The SPIOs contain an iron oxide core of 10 nm in diameter. Oleic acid shell, amphiphilic polymer coating and hydrated layer increased hydrodynamic size of SPIOs to 18.7 ± 5.1 nm (Figure 1). To reduce nonspecific binding with cell membranes and stabilize SPIOs, SPIOs were PEGylated using excess heterobifunctional PEG polymer (NH_2-PEG-COOH). The carboxyl groups on the surface of SPIOs were activated by EDC and sulfo-NHS and then covalently coupled to the primary amine of PEG by forming an amide bond. PEGylation of SPIOs resulted in a hydrodynamic size of 27.9 ± 7.7 nm but did not significantly change zeta-potentials (−35.3 mV vs −37.4 mV) (Table 1). The carboxyl group of PEG on SIPO surface was covalently linked to the amines of antibody and 5-FAM cadaverine through amide formation. SPIOs labeled with antibodies and 5-FAM showed increased hydrodynamic sizes (44.6 ± 20.3 nm for mAb-SPIOs and 43.5 ± 22.4 nm for IgG-SPIOs) and zeta-potentials (−26.1 mV for mAb-SPIOs and −25.5 mV for IgG-SPIOs). Agarose gel electrophoresis was utilized to characterize PEGylated SPIOs and nanoconjugates. It was found that mAb-SPIOs and IgG-SPIOs migrated more slowly than SPIOs and PEGylated SPIOs (Figure 2), indicating that mAb-SPIOs and IgG-SPIOs have larger sizes and smaller surface charges. Consistent with DLS measurement, PEGylated SPIOs migrated more slowly than SPIOs due to the increased particle size. The results from particle size and zeta-potential measurement as well as electrophoresis suggested that SPIOs were successfully PEGylated and labeled with antibodies.

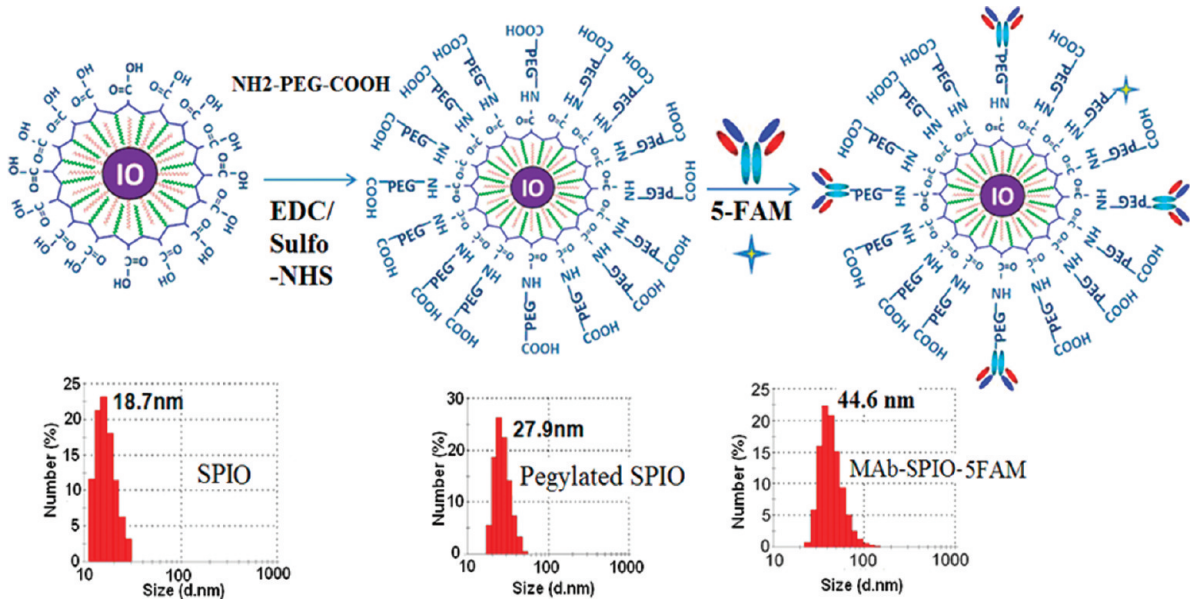

Figure 1. SPIO PEGylation and conjugation with antibody and 5-FAM.

Table 1. Zeta-Potential of SPIOs, PEGylated SPIOs, and Antibody-Labeled SPIOs

	zeta-potential (mV)
SPIOs	−37.4 ± 1.1
PEGylate SPIOs	−35.3 ± 0.8
IgG-SPIOs	−25.5 ± 2.9
mAb-SPIOs	−26.1 ± 3.4

mAb-SPIOs Target Cancer Cells (LS174T) by Fluorescence Microscopy, Prussian Blue Staining and MRI Scan. In the current study, fluorescence microscopy imaging, Prussian blue staining and MRI scan were used to test cancer cell targeting efficiency of SPIO conjugates. Figure 3 shows the fluorescent microscope images of LS174 cells (TAG-72 positive) after incubation with 5-FAM labeled SPIOs (A, B), IgG-SPIOs (C, D) and mAb-SPIOs (E, F). Figures 3G and 3H show the fluorescent images of A375 cells (TAG-72 negative) after incubation with mAb-SPIOs. The green fluorescence in Figures 3A, 3C, and 3E was from 5-FAM. Nuclei were stained in blue using Hoechst. The merged image (Figure 3F) shows that the incubation with mAb-SPIOs for 4 h resulted in binding and uptake of mAb-SPIOs to LS174T cells. However, the binding and uptake of nontargeted IgG-SPIOs (Figure 3D) and SPIOs (Figure

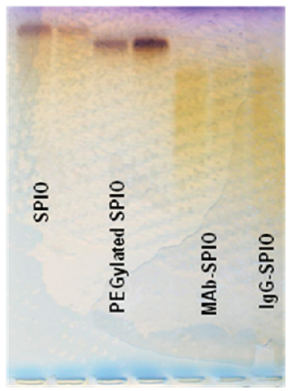

Figure 2. Migration of SPIOs, PEGylated SPIOs, and antibody-labeled SPIOs in agarose gel electrophoresis.

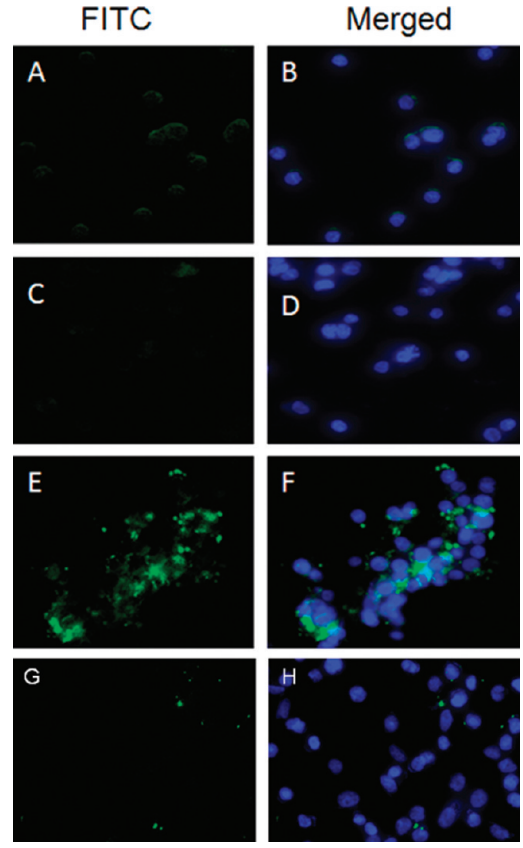

Figure 3. Fluorescent microscope images of LS174 cells after incubation with 5-FAM labeled SPIOs (A, B), nonspecific IgG-SPIO (C, D) and HuCC49ΔCH2-SPIOs (E, F) and A375 cells after incubation with HuCC49ΔCH2-SPIOs (G, H). Nuclei were stained with Hoechst.

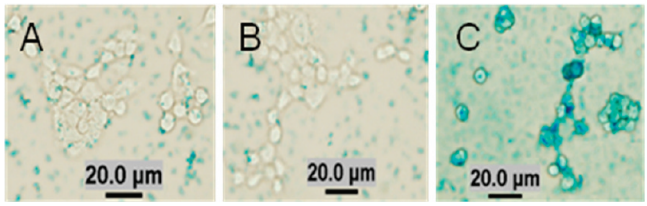

Figure 4. Prussian blue staining of LS174T cells incubated with SPIOs (A), nonspecific IgG labeled SPIOs (B), and HuCC49ΔCH2 labeled SPIOs (C).

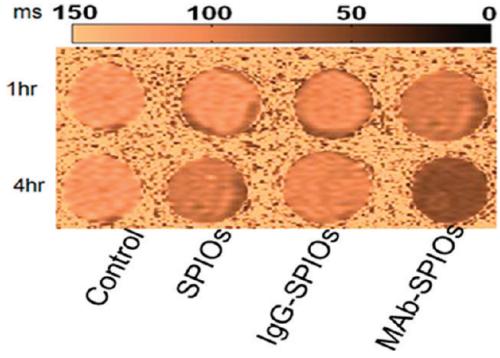

Figure 5. T_2-weighted spin−echo MR phantom images of LS174T cells incubated with SPIOs, nonspecific IgG labeled SPIOs, and HuCC49ΔCH2 labeled SPIOs.

Table 2. T_2 Relaxation Time of LS174T Cells Incubated with SPIOs and Antibody-Labeled SPIOs

	T_2 values (ms)	
	1 h incubation	4 h incubation
blank control	117.3 ± 1.8	118.9 ± 2.9
SPIOs	113.9 ± 4.6	91.9 ± 6.3
IgG-SPIOs	106.2 ± 4.5	100.9 ± 5.1
mAb-SPIOs	87.1 ± 3.7	55.5 ± 2.6

3B) were limited. Furthermore, mAb-SPIOs did not exhibit specific binding to A375 cells with low TAG-72 expression.

Figure 4 shows Prussian blue staining of LS174T cells incubated with SPIOs (A), nonspecific IgG labeled SPIOs (B), and HuCC49ΔCH2 labeled SPIOs (C). The blue color indicated the presence of SPIOs. The blue color in Figure 3C revealed that HuCC49ΔCH2 greatly improved the cancer cell targeting and uptake of SPIOs.

LS174T cells from the *in vitro* cellular uptake experiments were examined by MRI to evaluate the potential of mAb-SPIOs as a targeted MR contrast agent. The T_2-weighted MR phantom images of the cells incubated with SPIOs, IgG-SPIOs, and mAb-SPIOs, respectively, for 1 and 4 h are shown in Figure 5. The images of the cells incubated with mAb-SPIOs show a negative contrast enhancement (signal darkening) over other cells at both 1 and 4 h. Slight darkening was also observed for cells incubated with SPIOs and IgG-SPIOs when compared with control cells. T_2 transverse relaxation times of the samples were also measured, as shown in Table 2. All the nanoparticles exhibited a time-dependent uptake. More nanoparticle uptake was observed after 4 h incubation compared with 1 h incubation. LS174T cells incubated with mAb-SPIOs have much lower T_2 values (87.1−55.5 ms) than those incubated with SPIOs (113.9−91.9 ms) and IgG-SPIOs (106.2−100.9 ms), which is consistent with the increased mAb-SPIO uptake observed by fluorescence microscopy and Prussian blue staining.

Anticancer Drug Loading and pH-Dependent Release from SPIO Nanotheranostics. Four anticancer drugs, doxorubicin (Dox), azido-doxorubicin (Adox), MDM2 inhibitor (MI-219), and Hsp90 inhibitor (17-DMAG), were selected as the model drugs, and their structures are shown in Figure 6A. The four compounds have diverse lipophilicity. Dox is a liphophilic compound with a logP of 1.85.[10] The lipophilicity of Adox is further increased by attaching a lipophilic azide group. MI-219 is also a lipophilic compound. The predicted clogP of MI-219 by MarvinSketch was 3.12. In contrast, 17-DMAG is a hydrophilic compound with aqueous solubility of 1.4 mg/mL.[29]

Figure 6B shows the loading capacities (i.e., wt % of drug/SPIOs) of the four compounds. The data showed that 6.91 ± 0.47% of Adox, 3.85 ± 0.62% of Dox, 2.50 ± 0.31% of MI-219 and 0.1 ± 0.08% of 17-DMAG were encapsulated into SPIOs, suggesting that the loading capacity was correlated with lipophilicity of compounds. Compared with Dox, Adox has 1.8-fold loading capacity due to the replacement of NH_2 with azide group. The loading capacity of MI-219 was lower than that of Adox and Dox. When SPIOs were PEGylated and labeled with antibody, the loading capacities of Adox, Dox, MI-219 and 17-DMAG were 6.04 ± 0.61%, 3.16 ± 0.77%, 2.22 ± 0.42% and 0.09 ± 0.07%, which are similar to SPIOs. The hydrophilic PEG polymer and protein probably slightly affected the partitioning of drugs into the oleic acid shell, which is also observed in a previous study.[2]

Dox, MI-219 and 17-DMAG contain a primary amine, secondary amine, and tertiary amine, respectively, suggesting that the compounds can be protonated under various neutral or acidic pH values. In contrast, the azide of Adox cannot be protonated. Since protonation increases aqueous solubility of lipophilic drugs, the four compounds loaded in SPIOs are expected to exhibit different drug release profiles.

Figure 6C shows the percentages of released drugs in buffers of various pH in 1 h. Only 22.4% of Dox was released at pH 7.21. However, 55.5% of Dox was released at pH 5.66, and Dox was almost completely released at pH 3.20. In contrast, the release of Adox did not change significantly in either neutral or acidic buffers (only 17.6−33.4% of Adox was released at these conditions). In spite of the similar structure, Dox and Adox exhibited totally different release profiles, suggesting that the protonation of the primary amine resulted in the rapid release of Dox. MI-219 and 17-DMAG also showed pH-dependent release from SPIOs. More MI-219 and 17-DMAG were released when buffer pH decreased. Compared with Dox, comparable

(29) Tian, Z. Q.; Liu, Y.; Zhang, D.; Wang, Z.; Dong, S. D.; Carreras, C. W.; Zhou, Y.; Rastelli, G.; Santi, D. V.; Myles, D. C. Synthesis and biological activities of novel 17-aminogeldanamycin derivatives. *Bioorg. Med. Chem.* **2004**, *12* (20), 5317–5329.

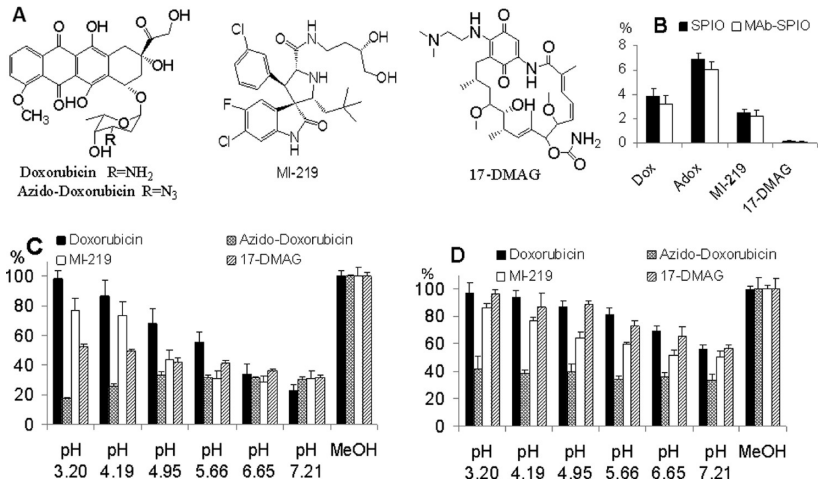

Figure 6. Anticancer drug loading capacities and pH-dependent release from SPIOs and HuCC49ΔCH2 labeled SPIOs. Structures of anticancer drugs (A); anticancer drug loading capacities of SPIOs and HuCC49ΔCH2 labeled SPIOs (B); percentages of released drug at various pH in 1 h (C) and 24 h (D).

percentages of MI-219 (30.7%) and 17-DMAG (31.7) were released at pH 7.21, but lower percentages were released at low pH buffers (77.0% of MI-219 and 52.1% of 17-DMAG were released at pH 3.20).

Figure 6D shows the percentages of drug release in buffers of various pH after incubation for 24 h. Compared with the incubation for 1 h, all four compounds exhibited increased release after 24 h, suggesting that the drug release from SPIOs was a dynamic process. The long-term incubation under low pH probably triggered the conformation changes and/or dissociation of polymers and oleic acid. Different from the other three compounds, the release of Adox was only slightly increased to 33.4−42.0% at various pH for 24 h, indicating that the release of Adox is not pH-dependent.

Intracellular Release of Dox and Adox from SPIO Nanotheranostics in Cancer Cells. Since Dox and Adox in SPIO nanotheranostics show different release profiles in buffers, Dox is expected to be released more rapidly than Adox after the nanotheranostics are internalized into the endosomes and lysosomes of cancer cells (LS174T). To visualize the intracellular release of Dox and Adox, LS174T cells were incubated with Dox-loaded SPIO nanotheranostics (Figure 7A) and Adox-loaded SPIO nanotheranostics (Figure 7C). These SPIO nanotheranostics were labeled with tumor targeting antibody (HuCC49ΔCH2) and fluorescent dye (5-FAM) in addition to loaded Dox or Adox.

The cells were imaged after incubation for 1 h (first row), 6 h (second row) and 24 h (third row). The images obtained with DAPI (first column), FITC (second column) and TRITC (third column) filters were overlaid to generate the merged images (fourth column). Green color showed the localization of 5-FAM labeled SPIO nanotheranostics. Nuclei were stained in blue color. Red color showed the distribution of Dox or Adox. The yellow color in the merged images indicated colocalization of 5-FAM-SPIOs and Dox or Adox. As a control, LS174T cells were also incubated with Dox alone (Figure 7B) and Adox alone (Figure 7D) for 1, 6, and 24 h.

As shown in Figure 7A, after incubation for 1 h, the cell membrane was stained with weak green fluorescence, indicating the binding of nanotheranostics to TAG-72 on the membrane. The red fluorescence from Dox also distributed on the membrane, and a small fraction of the Dox was released into the cells. After 6 h, the green fluorescence concentrated into bright dots, suggesting the accumulation of nanotheranostics in endosomes/lysosomes. The red fluorescence showed that Dox molecules were released from nanotheranostics and partitioned into cytosol, but the limited colocalization (weak yellow color in merged image) of SPIOs and Dox was still observed. After 24 h, almost all the green fluorescence localized in endosomes/lysosomes while most Dox accumulated in nucleus. As a comparison, the free Dox partitioned into cell cytosol in 1 h (Figure 7B), which was much faster than the Dox in SPIO nanotheranostics. Most free Dox localized in nuclei after incubation for 6 and 24 h.

In sharp contrast, when Adox-loaded SPIO nanotheranostics were incubated with LS174T cells, the staining pattern was different from that of Dox-loaded SPIO nanotheranostics. More colocalization of SPIOs and Adox was observed at 1 h (Figure 7C). After incubation for 6 and 24 h, most Adox-loaded SPIO nanotheranostics localized in endosomes/lysosomes. However, different from Dox, a bright yellow color in the merged images was observed, indicating the colocalization of SPIOs and Adox in endosomes/lysosomes. This suggest that most Adox was not released from lysosome even at the low pHs, and only a fraction of Adox partitioned into cytosol even after 24 h. Figure 7D shows the images of cells incubated with free Adox. Compared with Dox, the amount of Adox in nuclei was much lower even after 24 h, which was also observed in cells incubated with Adox-loaded SPIO nanotheranostics (Figure 7C).

Targeted SPIO Nanotheranostics Increase Cytotoxicity. Dox-loaded SPIO nanotheranostics (HuCC49ΔCH2 targeted) demonstrated a dose-dependent cytotoxicity with IC_{50} of 0.44 μM in LS174T cells (Figure 8A), which is lower than that of Dox-loaded SPIO nanotheranostics (nontargeted) with IC_{50}

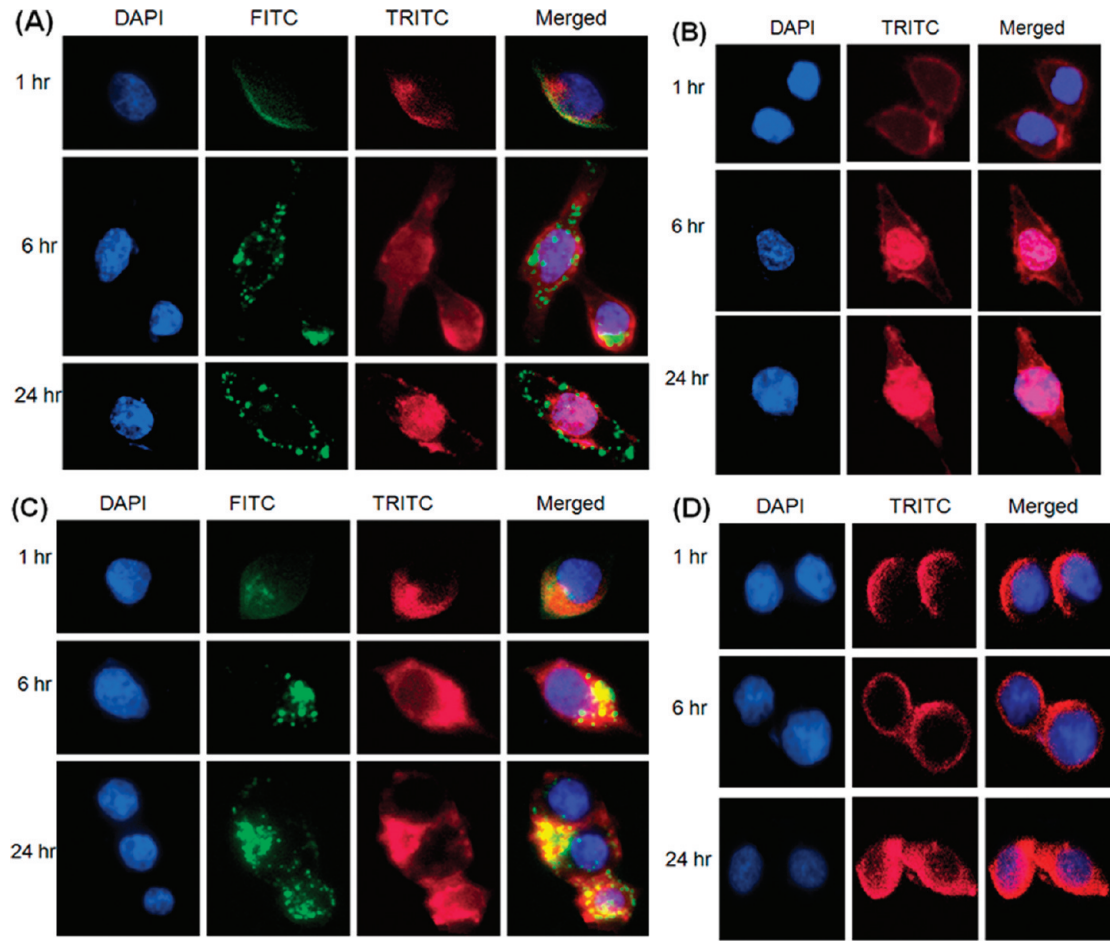

Figure 7. Intracellular distribution of doxorubicin (Dox), azido-doxorubicin (Adox), and HuCC49ΔCH2-SPIOs in LS174T cells. Fluorescent images of cells incubated with Dox (A); HuCC49ΔCH2-SPIOs loaded with Dox (B); Adox (C); and HuCC49ΔCH2-SPIOs loaded with Adox (D). Green color shows the localization of SPIOs (5-FAM). Nuclei are stained in blue color. Red color shows the distribution of Dox or Adox. The yellow color in the merged images indicates colocalization of SPIOs and Dox or Adox.

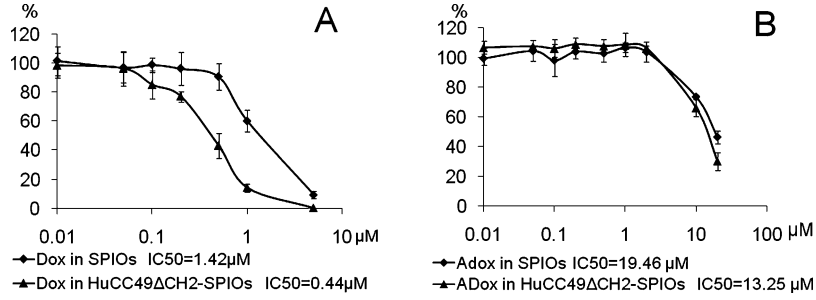

Figure 8. Antiproliferation activity of Dox-loaded HuCC49ΔCH2-SPIOs (A) and Adox-loaded HuCC49ΔCH2-SPIOs (B) on LS174T cells.

of 1.42 μM. These data suggest that targeted nanotheranostics delivered Dox into cancer cells and Dox is released from SPIO nanotheranostics for anticancer activity.

In contrast, Adox with an azide group was less potent than Dox. When Adox was encapsulated into SPIO nanotheranostics, the IC_{50} was 19.46 μM (nontargeted) and 13.25 μM (targeted). No significant difference was observed. These data suggested that Adox was not efficiently released from nanotheranostics even if they were target-delivered to cancer cells. As a control, 0.1 mg/mL of SPIOs without drugs were incubated LS174T cells and no inhibition on cell growth was observed (data not shown).

Discussion

The stability of amphiphilic polymer coated SPIOs in aqueous solution was maintained by the electrostatic repulsion between the negatively charged SPIOs. To avoid agglomeration, it is critical to maintain the electrostatic repulsion during conjugation of antibody and 5-FAM. SPIO agglomeration was observed when 5-FAM cadaverine was

added to SPIOs (pH 5.5) activated by EDC and sulfo-NHS. The agglomeration was probably caused by the positive charges of 5-FAM cadaverine since the amines of cadaverine were protonated at pH 5.5. To reduce the positive charges, 5-FAM cadaverine was dissolved in 30 mM borax solution (pH 9.1) and then added to the activated SPIOs. The pH of the mixed solution was adjusted to >8.0, an optimal pH for EDC-mediated coupling reactions.[30] Positive charges of 5-FAM cadaverine were minimized at pH >8, and no agglomeration was observed. Meanwhile, the mass ratio of 5-FAM cadaverine and SPIOs was reduced to 1:10 to avoid agglomeration. Additionally, the surface conjugation with proteins such as antibody[31,32] and scFv fragment[33] has been reported to be able to stabilize nanoparticles due to steric stabilization. Hence, antibody was first added to the activated SPIOs to stabilize the SPIOs, and 5-FAM cadaverine was added 5 min later. By using this method, stable mAb-SPIOs, IgG-SPIOs and SPIO-5FAM conjugates were prepared. Although 5-FAM and antibody labeling increased zeta-potentials of the conjugates, the nanoconjugates still exhibited low zeta-potentials (−25 to −26 mV) under which there was enough electrostatic repulsion to prevent flocculation.

Although SPIOs can be accumulated in tumors through the EPR effect[1] or by applying an external magnetic field,[6,34] coupling SPIOs with antibodies or targeting molecules could be an approach to deliver the SPIOs and drugs more effectively.[2−4] Tumor associated glycoprotein 72 (TAG-72) is a human mucin like glycoprotein complex, which is overexpressed in many epithelial-derived cancers.[35] HuCC49Δ-CH2 is a humanized C_H2 domain-deleted anti-TAG-72 monoclonal antibody. Compared with murine CC49 antibody, the humanized antibody will overcome the immunogenicity problem in clinical investigation and the deletion of C_H2 domain will decrease the size of nanoconjugates. Our previous studies[25,36] showed that HuCC49ΔCH2 could specifically bind to LS174T colon cancer cells which had overexpression of TAG-72. The *in vitro* binding studies by fluorescence microscopy, Prussian blue staining and MRI scan showed the specific targeting of the HuCC49ΔCH2 labeled SPIOs (mAb-SPIOs) in LS174T colon cancer cells in comparison with SPIOs and IgG-SPIOs.

SPIOs have been widely used as a negative contrast agent for MRI. Different sizes of SPIOs can lead to different magnetic properties. For instance, size dependent MR signal is in the range of 4−12 nm, where a continual decrease in the T_2-weighted MR signal intensity correlated with the increase of the size of SPIOs.[21,37] Hence, we chose SPIOs with an iron oxide core of 10 nm in diameter for cancer cell imaging and drug delivery. The T_2-weighted phantom images of LS174T cells showed that the SPIOs could effectively decrease T_2 relaxation time of cancer cells incubated with mAb-SPIOs, suggesting that it is feasible to use the nanoconjugate as an MRI contrast agent to image the tumors and monitor drug delivery.

The iron oxide core of SPIOs is coated with a lipophilic oleic acid shell and an outer surface of amphiphilic polymer. Lipophilic molecules are expected to penetrate the polymer surface and distribute into the oleic acid shell. Hence, the drug loading capacities are found to be correlated with the lipophilicity of the drugs. In this study, the loading capacity of Dox was determined as 3.85 wt %. Various Dox loading capacities into SPIOs have been reported such as 2%,[1] 2.3%,[2] and 3.7−8.2%.[8,10] The variation of Dox loading capacities may be caused by the weight percentage of oleic acid in the SPIOs, particle size, the amount of added Dox and the separation process. For example, 5 nm SPIOs were found to have a slightly higher Dox loading capacity than 10 nm SPIOs[2] due to the higher surface area/weight ratio or higher percentage of oleic acid. The weight ratio of added Dox and SPIOs may affect the drug loading. Since the electrostatic interaction between amine of Dox and carboxyl of SPIOs may change the zeta-potential of SPIOs and probably result in flocculation, a low weight ratio of added Dox and SPIOs of 1:3 was used as previously reported.[2] LC−MS/MS assays were used to quantify the four anticancer drugs in this study, which led to accurate and reliable estimations of drug loading capacity and release profile. LC−MS friendly acetic acid/ammonium acetate/ammonium hydroxide buffer was used for drug loading and release.

pH-dependent release of Dox from nanoparticles has been previously reported,[2,4,7,12] which has been explained by the

(30) Grabarek, Z.; Gergely, J. Zero-Length Crosslinking Procedure with the Use of Active Esters. *Anal. Biochem.* **1990**, *185* (1), 131–135.

(31) Watanabe, H.; Nakanishi, T.; Umetsu, M.; Kumagai, I. Human anti-gold antibodies: Biofunctionalization of gold nanoparticles and surfaces with anti-gold antibodies. *J. Biol. Chem.* **2008**, *283* (51), 36031–36038.

(32) Pissuwan, D.; Cortie, C. H.; Valenzuela, S. M.; Cortie, M. B. Gold nanosphere-antibody conjugates for hyperthermal therapeutic applications. *Gold Bull.* **2007**, *40* (2), 121–129.

(33) Liu, Y.; Liu, Y.; Mernaugh, R. L.; Zeng, X. Q. Single chain fragment variable recombinant antibody functionalized gold nanoparticles for a highly sensitive colorimetric immunoassay. *Biosens. Bioelectron.* **2009**, *24* (9), 2853–2857.

(34) Kumar, A.; Jena, P. K.; Behera, S.; Lockey, R. F.; Mohapatra, S.; Mohapatra, S. Multifunctional magnetic nanoparticles for targeted delivery. *Nanomedicine* **2010**, *6* (1), 64–69.

(35) Johnson, V. G.; Schlom, J.; Paterson, A. J.; Bennett, J.; Magnani, J. L.; Colcher, D. Analysis of a Human Tumor-Associated Glycoprotein (Tag-72) Identified by Monoclonal-Antibody B72.3. *Cancer Res.* **1986**, *46* (2), 850–857.

(36) Xiao, J.; Horst, S.; Hinkle, G.; Cao, X.; Kocak, E.; Fang, J.; Young, D.; Khazaeli, M.; Agnese, D.; Sun, D.; Martin, E., Jr. Pharmacokinetics and clinical evaluation of 125I-radiolabeled humanized CC49 monoclonal antibody (HuCC49deltaC(H)2) in recurrent and metastatic colorectal cancer patients. *Cancer Biother. Radiopharm.* **2005**, *20* (1), 16–26.

(37) Jun, Y. W.; Huh, Y. M.; Choi, J. S.; Lee, J. H.; Song, H. T.; Kim, S.; Yoon, S.; Kim, K. S.; Shin, J. S.; Suh, J. S.; Cheon, J. Nanoscale size effect of magnetic nanocrystals and their utilization for cancer diagnosis via magnetic resonance imaging. *J. Am. Chem. Soc.* **2005**, *127* (16), 5732–5733.

protonation of the NH_2 group of Dox under low pH,[2] weakened interaction between Dox and the partially neutralized carboxyl groups,[4] and conformation change of amphiphilic polymers or oleic acid.[21] In this study, Dox and Adox exhibited dramatically different release profiles in terms of both rate and extent. Furthermore, MI-219 and 17-DMAG, which can be protonated at low pH, also exhibited pH triggered release. The results suggested that protonation plays a major role in drug release at low pH. It was observed that more drugs were released from SPIOs after incubation for 24 h, indicating that the conformation change or dissociation of amphiphilic polymers and oleic acid may also contribute to the drug release. Although 17-DMAG has an aqueous solubility of 1.4 mg/mL and a very low loading capacity, it was not totally released even at pH 3.20, implying the existence of other interactions between 17-DMAG and SPIOs (i.e., electrostatic interaction).

It has been reported that SPIOs are normally taken up by cells via endocytosis into phagosomes, which then eventually fuse with lysosomes for degradation.[38] Due to the acidic environment in endosomes and lysosomes, Dox and Adox were expected to show different release profiles. A fluorescent microscope was used to visualize the intracellular release of Dox and Adox from SPIOs. The very limited colocalization of Dox and 5-FAM-SPIOs in endosomes/lysosomes at 6 h suggested that most Dox were released from SPIOs and escaped into cytosol, which was consistent with the drug release observed in various pH buffers. For Adox release, the colocalization of 5-FAM-SPIO and Adox indicates that the release rate of Adox in endosomes/lysosomes was much slower than that of Dox. It is not surprising to observe the low accumulation of Adox in nuclei even after incubation with either Adox-loaded mAb-SPIOs or free Adox for 24 h. The amino sugar residue, especially the amine group, was reported[39,40] to be necessary to maintain the maximum van der Waals contact between Dox and DNA base pairs.

MTS assays showed that HuCC49ΔCH2 labeled SPIO nanotheranostics could increase the cytoxicity of Dox by more than 3-fold (IC_{50} 1.42 μM vs 0.44 μM) compared to nontargeted SPIO nanotheranostics. This suggests that HuCC49ΔCH2 labeled SPIO nanotheranostics were targeted to cancer cells and internalized, and drug was released to achieve the anticancer effect. In contrast, the nontargeted SPIO nanotheranostics which did not bind to cancer cells were not efficiently internalized, and the drug was not efficiently released in the cell culture medium at pH 7.4. However, when SPIO nanotheranostics were loaded with Adox, the targeted SPIO nanotheranostics did not improve its efficacy compared to nontargeted ones, which suggested that Adox was not efficiently released intracellularly even when the nanotheranostics were internalized into cancer cells.

In summary, we prepared targeted SPIO nanotheranostics, which were labeled with fluorescence dye and TAG-72 targeting antibody, and loaded with anticancer drugs for both cancer cell imaging and anticancer drug delivery. The SPIO nanotheranostics could specifically target to LS174T colon cancer cells for fluorescent cancer imaging and effectively decrease the T_2 relaxation times in MR imaging. Four anticancer drugs (doxorubicin, azido-doxorubicin, MI-219 and 17-DMAG) were encapsulated into SPIO nanotheranostics and exhibited pH-dependent release in cancer cells, resulting in an improved anticancer efficacy. These targeted nanotheranostics provide an integrated platform for targeted drug delivery, cancer imaging and visualization of drug release.

Acknowledgment. This work was partially supported by the National Institutes of Health (RO1 CA120023, and R21 CA143474); University of Michigan Cancer Center Research Grant (Munn); and University of Michigan Cancer Center Core Grant to D.S.

MP100273T

(38) Schwalbe, M.; Jorke, C.; Buske, N.; Hoffken, K.; Pachmann, K.; Clement, J. H. Selective reduction of the interaction of magnetic nanoparticles with leukocytes and tumor cells by human plasma. *J. Magn. Magn. Mater.* **2005**, *293* (1), 433–437.

(39) Yan, Q.; Priebe, W.; Chaires, J. B.; Czernuszewicz, R. S. Interaction of doxorubicin and its derivatives with DNA: Elucidation by resonance Raman and surface-enhanced resonance Raman spectroscopy. *Biospectroscopy* **1997**, *3* (4), 307–316.

(40) Bailly, C.; Qu, X. G.; Anizon, F.; Prudhomme, M.; Riou, J. F.; Chaires, J. B. Enhanced binding to DNA and topoisomerase I inhibition by an analog of the antitumor antibiotic rebeccamycin containing an amino sugar residue. *Mol. Pharmacol.* **1999**, *55* (2), 377–385.